Electrochemical CO_2 Reduction on Polycrystalline Copper by Modulating Proton Transfer with Fluoropolymer Composites

Hanqing Pan and Christopher J. Barile*

Department of Chemistry, University of Nevada, Reno, Nevada 89557, USA

*Corresponding author: cbarile@unr.edu

Keywords: CO_2 reduction, proton transfer, electrocatalysis, membranes, fluoropolymers

Abstract

Electrochemical reduction of CO_2 to alcohols and hydrocarbon fuels offers a sustainable pathway towards mitigating atmospheric CO_2 while concomitantly generating value-added products. Our group recently demonstrated that Nafion-modified electrodes give an extraordinarily high yield of CH_4 (Faradaic efficiency of 88% at -0.4 V vs. RHE at room temperature) through the stabilization of a metal-bound CO intermediate. In this work, we fabricate Cu electrodes with a polymer blend of Nafion and polyvinylidene fluoride (PVDF) to modulate proton transfer to the metal-CO intermediate. Electrodes modified with hydrophobic PVDF blended into Nafion generate high yields of formate (Faradaic efficiency of 58% at -0.15 V vs. RHE). In addition, the total proton concentration in the electrolyte is decreased by adding an aprotic solvent to slow down proton transfer rates at the electrode-polymer interface. This control over proton transfer rate results in higher yields of C2+ products including ethylene, ethanol, and 1-propanol. We demonstrate that a Cu electrode with a 15 μm Nafion overlayer in an acetonitrile/bicarbonate electrolyte results in a higher yield of total carbon-containing products than an analogous unmodified Cu electrode. The total yield of carbon-containing products on these electrodes is as high as nearly 100%, indicating that hydrogen evolution does not occur under properly controlled conditions. Taken together, these results demonstrate how the selectivity of Cu-based CO_2 reduction electrocatalysts can be tuned by controlling proton transfer dynamics.

Introduction

Electrochemical CO_2 reduction to fuels is a promising method of mitigating climate change. Despite intensive research efforts over the last decade, this approach is still impractical from a technological standpoint. Though state-of-the-art Cu-based CO_2 reduction catalysts are capable of producing C2 and C3 products,[1-14] superior Cu CO_2 reduction catalysts must be developed because Faradaic efficiencies are often low, resulting in poor catalyst selectivity and the H_2 evolution reaction (HER).[15-18] This poor selectivity coupled with the limited solubility of CO_2 in water[19,20] and the high overpotentials needed to achieve appreciable reaction kinetics, demonstrate that superior CO_2 reduction electrocatalysts are needed in order for practical CO_2 conversion devices to become a reality.

For these reasons, the fabrication of novel CO_2 reduction electrodes with high durability and selectivity towards carbon-containing products is a grand challenge. Methods for designing these electrodes include tuning the morphology of the catalyst,[21-25] surface modification,[26-29] alloying multiple metals,[30-33] controlling the pH at the electrode-electrolyte interface,[34-37] utilizing non-aqueous solvents,[38-42] and controlling proton and electron transfer rates.[43-45] For example, Dinh *et al*. were able to convert CO_2 to ethylene with a high Faradaic efficiency of 70% at -0.55 V vs. RHE using a Cu electrode in alkaline media. They proposed that the hydroxide ions on or near the Cu surface lower the CO_2 reduction and CO-CO coupling activation energy barriers.[46] Similarly, Huo and co-workers prepared Cu particles supported by nitrogen-doped carbon frameworks capable of converting CO_2 to ethylene (Faradaic efficiency of 63.7%) due to synergistic interactions between nitrogen dopants and stepped surface-rich Cu particles.[47] Mistry *et al*. developed oxidized Cu catalysts exhibiting low overpotentials for CO_2 electroreduction and high selectivity for ethylene (Faradaic efficiency of 60%).[48] Finally, a lesser-known strategy is to

control the hydrophobicity of the electrode to tune product selectivity. Studies have shown that submerged hydrophobic surfaces can trap gas at the nanoscale,[49,50] which allows for CO_2 to accumulate at the electrode-electrolyte interface and improve product selectivity.

Hydrophobic polymers and organic molecules have been previously used to modify metal CO_2 reduction electrodes. Sakamoto *et al*. coated an Ag electrode with polystyrene microspheres, which enhanced CO production while suppressing H_2 evolution.[51] Buckley and co-workers reported the ability to alter the CO_2 reduction selectivity of a Cu electrode by modifying the surface with protic, hydrophilic, and cationic hydrophobic species. It was found that protic species enhance selectivity for H_2, hydrophilic species enhance formic acid, and cationic hydrophobic species enhance CO selectivity.[52] Li *et al*. designed an electrode with hydrophobic nanoporous polyethylene membranes that resulted in a high CO production Faradaic efficiency of 92%.[53] Wakerley *et al*. created a superhydrophobic surface by treating Cu dendrites with 1-octadecanethiol. This hydrophobic electrode achieved up to 56% Faradaic efficiency for ethylene and 17% for ethanol at neutral pH, compared to 9% and 4% on its analogous hydrophilic electrode.[54]

Along these lines, our group previously demonstrated that Nafion-modified Cu electrodes give an extraordinarily high yield of CH_4 (Faradaic efficiency of 88% at -0.4 V vs. RHE at room temperature) through the stabilization of a metal-bound CO intermediate.[43] To the best of our knowledge, this Faradaic efficiency for CH_4 is the highest achieved under ambient conditions. As a result of this previous work, we hypothesize that it is possible to generate C2 and C3 products by slowing down proton transfer to the M-CO intermediate to lower the yield of CH_4 and instead increase M-CO coupling chemistry. Slowing down proton transfer could be achieved by changing

the hydrophobicity of the polymer overlayer and/or changing the proton availability in bulk solution.

In this work, we report the construction of Cu electrodes modified with PVDF-Nafion polymer overlayers to control the hydrophobicity of the electrode and demonstrate that hydrophobicity is a governing factor of product selectivity in electrochemical CO_2 reduction. A hydrophobic environment enhances formate selectivity because formate is the only CO_2 reduction product that does not generate water as a coproduct as a hydrophobic environment renders water formation unfavorable. We also decreased the total proton concentration in the electrolyte by adding an aprotic solvent (acetonitrile) to the bicarbonate electrolyte. Less proton availability slows down proton transfer to the M-CO intermediate and results in the formation of C2 and C3 products such as ethylene, ethanol, and 1-propanol.

Experimental section

Materials and electrode preparation. A Nafion D520 dispersion was purchased from Fuel Cell Store. Cu foil (99.99% purity) was purchased from All-Foils, Inc. CO_2 and CO were purchased from Airgas. Acetonitrile was purchased from Fisher Chemical. Sodium bicarbonate and polyvinylidene fluoride were purchased from Sigma Aldrich. Nafion/PVDF polymer blends were made by mixing various ratios (4, 8, 15, 30, 52, 56, 60, 64, 68 and 100 wt. %) of PVDF into Nafion. The mixtures were then sonicated for 30 minutes to allow for the complete dispersion of PVDF into Nafion. Nafion/PVDF-modified electrodes were fabricated by drop-casting the polymer dispersions directly onto the substrate and subsequently letting the films dry in air.

Electrochemical Measurements and Material Characterization. All electrochemical measurements were performed using a VSP-300 Biologic Potentiostat. All electrochemical data were collected versus a Ag/AgCl reference electrode and converted to the reversible hydrogen

electrode (RHE) scale by $V_{(vs.\ RHE)} = V_{(measured\ vs.\ Ag/AgCl)} + 0.21 + 0.059*6.8$ (where 6.8 is the pH of solution). All values are reported versus RHE. Current densities are reported with respect to the geometric area of the working electrode. For linear sweep voltammogram studies, the geometric working electrode area was 0.22 cm^2 and for all other experiments, the geometric working electrode area was 5.0 cm^2. To evaluate the CO_2 reduction activity of the thin films, the working electrodes were studied in 0.1 M sodium bicarbonate buffer sparged with CO_2 gas for at least 30 min using a one-compartment, three-electrode configuration. Scanning electron microscope (SEM) images and energy-dispersive X-ray (EDS) analysis were obtained for each sample using a JEOL JSM-6010LA analytical SEM or a JEOL JSM-7100F field emission SEM operated using an accelerating voltage of 15 kV. Onset potentials were calculated by determining the voltage at which the current density reached 15% of the maximum current density for each linear sweep voltammogram. Contact angle measurements were acquired using a Rame-Hart 100-00 goniometer. Distilled water (30 µL) was transferred onto each electrode surface using a pipette and the measurement was taken after 5 seconds. The water contact angles were measured at ambient temperature. The left and right angles were measured and averaged, and measurements for each sample were triplicated.

Product Determination. Electrochemical reactions were performed chronoamperometrically at -0.89 V vs. RHE (and at -0.38 V, -0.13 V, and 0.12 V vs. RHE for voltage-dependent experiments) for one hour using carbon as a counter electrode in a beaker for determining liquid and solid products and Pt wire as a counter electrode in a custom-made cell for determining gas products. During chronoamperometry, CO_2 was continuously sparged through the solution (2.5 mL) at a rate of 5 cm^3/min. Liquid products were quantified using a Varian 400 MHz NMR Spectrometer using DMF as an internal standard. After chronoamperometry, the water in the reaction solution was

evaporated under reduced pressure, and sodium formate along with other residual solids from the electrolyte were collected and dissolved in D_2O. Liquid products were extracted from the reaction solution using deuterated chloroform. Gas products were quantified using a SRI 8610C gas chromatograph equipped with a flame ionization detector (FID) and a methanizer. The limits of detection for formate, liquid products, and gas products were determined to be 11 μM, 85 μM, and 1 ppm, respectively. Liquid products in acetonitrile/bicarbonate electrolyte were analyzed by an Agilent Technologies GC-MS instrument equipped with a 7890A GC system and 5975C inert MSD with a Triple-Axis Detector. The limits of detection for methanol, ethanol, and 1-propanol were 5 μM. All experiments were at least duplicated, and all error bars presented are the standard deviation among the multiple trials.

Results and Discussion

Surface Characterization of Cu Electrocatalysts Modified with Nafion-PVDF Blends

To characterize the surface of the polymer-modified electrodes, we first collected a cross-sectional scanning electron microscopy (SEM) image of a Cu electrode modified with a PVDF-Nafion polymer overlayer (Fig. 1A). Energy-dispersive X-ray (EDS) analysis was also carried out to confirm the uniformity of the polymer overlayer and elemental composition of the electrode. The EDS results reveal that F and O, which are components of Nafion and PVDF, are fairly uniformly distributed on top of the Cu electrode (Figs. 1B-D).

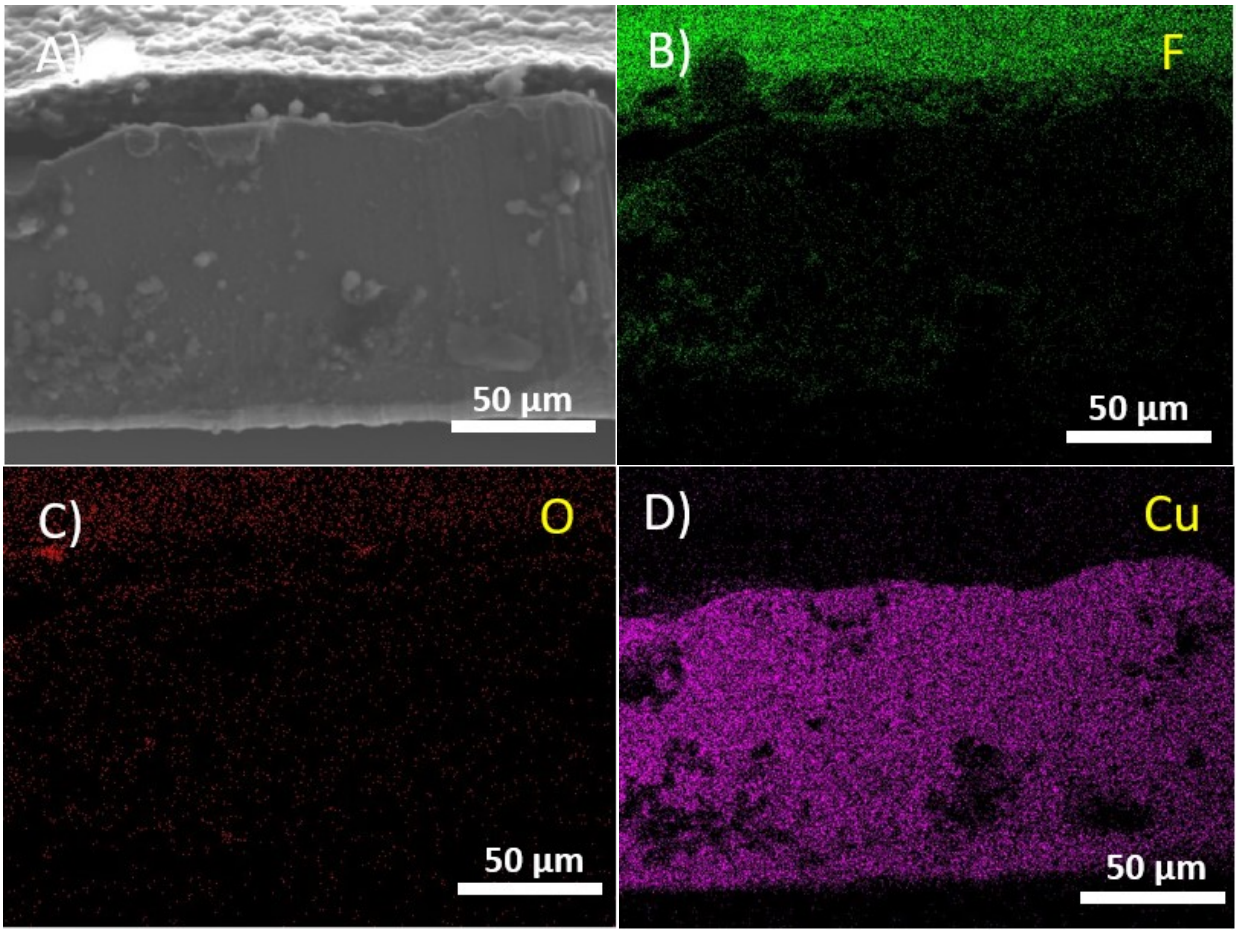

FIGURE 1. Cross-sectional SEM image (A) and EDS elemental mapping of F (B), O (C) and Cu (D) of a Cu electrode modified with a PVDF-Nafion polymer overlayer.

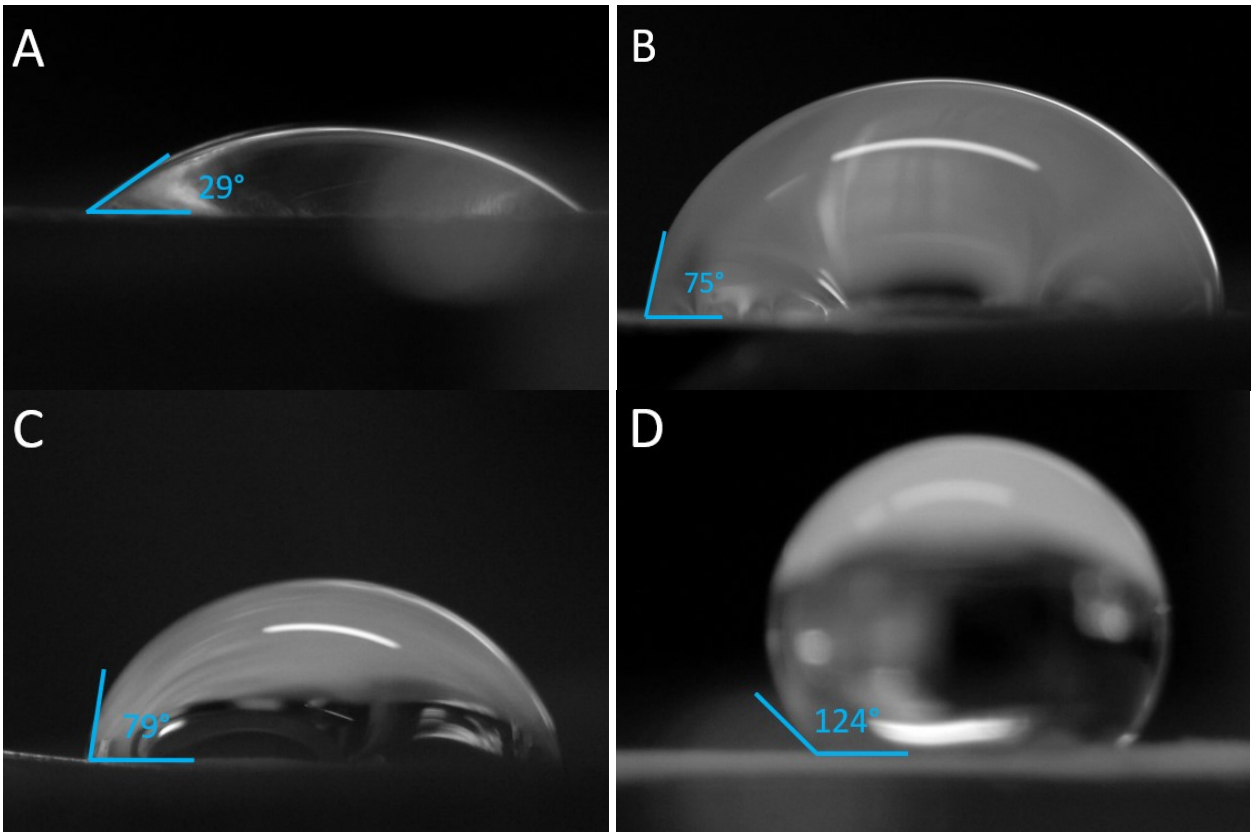

FIGURE 2. Photographic images showing the contact angle of a water droplet on a bare Cu electrode (A) and Cu electrode modified with Nafion-PVDF overlayers containing 30 wt. % (B), 52 wt. % (C) and 100 wt. % (D) PVDF.

Contact angle measurements were conducted to compare the hydrophobicity change when Cu is modified by PVDF-Nafion overlayers with increasing amounts of PVDF. On a bare Cu electrode, the angle of contact between the water droplet to the electrode surface is 29°. When the Cu electrode is modified with a PVDF-Nafion overlayer, the contact angle consistently increased from 38° (4 wt. % PVDF) to 124° (100 wt. % PVDF) with increasing weight percent of PVDF (Figs. 2A-D, Table S1). The increase in contact angle with PVDF concentration corresponds to the increased hydrophobicity of the electrode due to the inclusion of hydrophobic PVDF in the composite overlayer. After CO_2 reduction catalysis, the contact angles of all of the electrodes, including unmodified Cu, change from their original values.

CO_2 Reduction by Cu Electrocatalysts Modified with PVDF-Nafion

Linear sweep voltammetry was performed on a bare Cu electrode and Cu electrodes modified with Nafion and PVDF-Nafion blend overlayers (Fig. 3). The addition of a Nafion overlayer causes a positive shift in the onset potential of the CO_2 reduction reaction. The unmodified Cu electrode exhibits an onset potential (defined as the potential at which 15% of the maximum cathodic current measure during the voltammetry is reached) of -0.19 V vs. RHE compared to +0.40 V vs. RHE for the Cu electrode modified with 15 μm of Nafion (black and red lines, respectively). A Cu electrode modified with a 60 wt. % PVDF-Nafion blend overlayer possesses an onset potential of +0.37 V vs. RHE (green line), a value which is also positive compared to unmodified Cu, but negative compared to that of the Cu electrode with a pure Nafion overlayer. Furthermore, when a Cu electrode is modified with 100 wt. % PVDF, it exhibits almost zero current density (purple line) due to the electronically and ionically insulating nature of PVDF. Indeed, the charge transfer resistance, as calculated from electrochemical impedance spectroscopy, of the 100 wt. % PVDF electrode (1.5 MΩ) is dramatically higher than the electrodes with lower PVDF loadings (0.4-2.3 kΩ, Table S2). Taken together, these results indicate that increasing amounts of PVDF in the fluoropolymer overlayer shift the catalytic CO_2 reduction current to more negative potentials. We note that the +0.40 V vs. RHE and +0.37 V vs. RHE onset potentials calculated for the membrane-modified electrodes are more positive than the standard reduction potentials for CO_2 reduction reactions.[55] These onset potentials are reported vs. RHE assuming a pH of 6.8, which is the pH of the bulk solution. However, the pH at the Cu-Nafion interface where the reaction occurs is not the same as the bulk solution pH. Because Nafion is a superacid[56] with an approximate pK_a of -6, the interfacial pH is much lower than 6.8, which shifts these onset potentials to more negative values vs. RHE according to the Nernst equation.

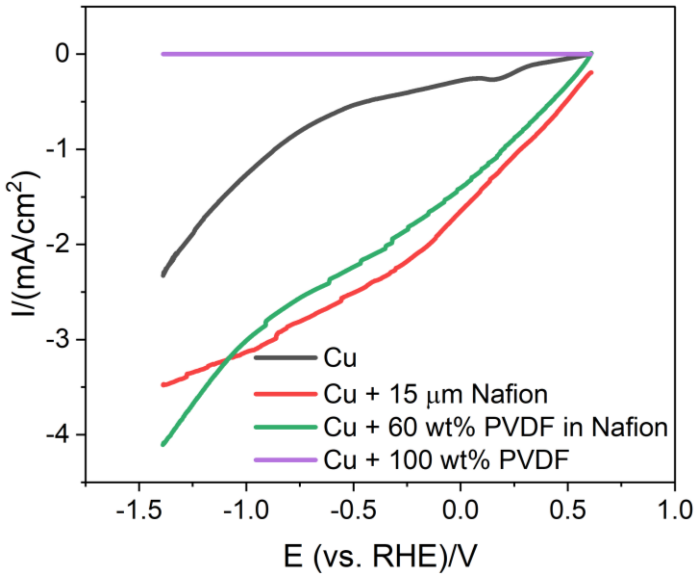

FIGURE 3. Linear sweep voltammograms (LSV) of bare Cu (black), Cu modified with 15 μm Nafion (red), Cu modified with 60 and 100 wt. % PVDF in Nafion overlayer (green and purple, respectively) in CO_2-saturated 0.1 M $NaHCO_3$ electrolyte at a scan rate of 10 mV/s.

Moreover, the changes in the voltammetry with different polymer overlayers are reflective of changes in the CO_2 reduction process as evidenced by product analysis conducted using chronoamperometry over the course of 1 hour (Fig. S1). When a Cu electrode is modified by PVDF-Nafion polymer overlayers, the production of CO, HCOOH, and CH_4 is hindered at PVDF weight percentages greater than 8% (Fig. 4A). Previously, we found that a bare Cu electrode yields 24% CO and 23% formate,[43] and no CH_4 is produced at -0.89 V vs. RHE. With a 0 wt. % PVDF (pure Nafion overlayer), a high CH_4 yield is achieved (68%) (Fig. 4A). This high CH_4 yield is attributed to the stabilization of the metal-bound CO intermediate (M-CO) by Nafion that allows for the subsequent rapid protonation of the intermediate to produce CH_4.[43] Adding 4 wt. % PVDF significantly hinders CH_4 production (14%) and beyond that loading, CH_4 production is not observed at all (Fig. 4A). Analysis of partial charge densities and rates of formation shows the same trends as observed for Faradaic efficiency (Fig. S4 and Fig 4B).

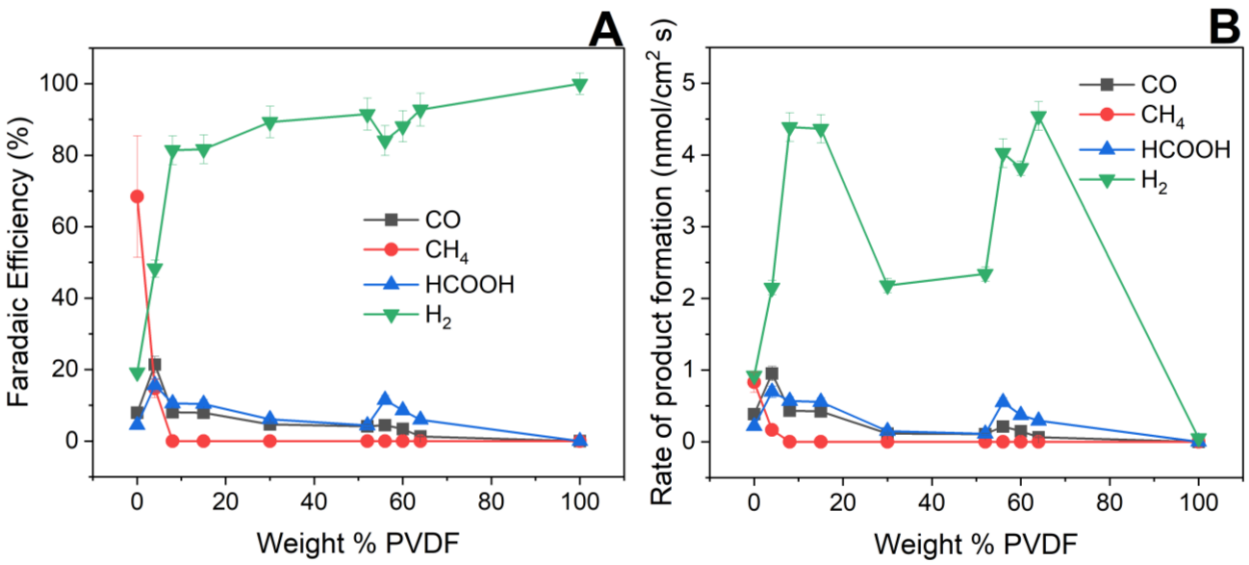

FIGURE 4. Faradaic efficiencies (A) and rate of formation (B) over the 1 hour experiment for formate, CO, and CH_4 produced from 20-90 µm PVDF-Nafion-modified Cu at -0.89 V vs. RHE. The PVDF-Nafion overlayer becomes increasingly thick as the weight percentage of PVDF increases.

We evaluated the product distribution of the electrode modified with 52 wt. % PVDF under varying voltages (Fig. 5). From Fig. 4, no CH_4 is produced at concentrations above 4 wt. % PVDF in the polymer overlayer. However, increasing to a much more negative voltage of -1.4 V vs. RHE generates 47% CH_4 (Fig. 5A). A similar trend is observed for CO. Minimal CO is produced until -1.4 V vs. RHE at which point the Faradaic efficiency is 15%. Interestingly, formate production reaches a maximum of 58% at -0.14 V. At 0.11 V, -0.14 V, and -0.39 V, formate production remains high, but decreases drastically at -0.89 V. This set of data indicates that formate production is preferred at a lower voltage, suggesting that formate production proceeds through a different mechanism than CO and CH_4. We hypothesize that this electrode yields high amounts of formate due to the hydrophobicity of the electrode. Formate becomes the preferred product using a hydrophobic interface because formate is the only CO_2 reduction product that does not also produce H_2O, and H_2O is unfavorable to generate in a hydrophobic environment. Compared to bare Cu, more formate is produced at a lower voltage,[57] but on Nafion-modified Cu, formate

production slowly increases at increasingly negative voltages.[43] While Toma et al.[58] determined that hydrophilic membranes promote formate production, the membranes used in that work were of nanometer thicknesses as opposed to the micron-thick membranes used here. Since we have demonstrated formate is the preferred product in more hydrophobic electrodes, one may wonder about the possibility of optimizing another electrode possessing a greater weight percent PVDF in the polymer overlayer, but mass transport calculations show that at or above 56 wt. % PVDF, CO_2 mass transport to the electrode surface begins to become a limiting factor (*vide infra*). Analysis of partial charge densities and rates of formation shows that CO, CH_4, and HCOOH production is highest at -1.4 V vs. RHE (Fig. S5 and Fig. 5B). We note that HCOOH and H_2 are produced even at the most positive voltage of 0.11 V vs. RHE. Although this voltage is more positive than the standard reduction potentials[55] for HCOOH and H_2 formation, as mentioned in our previous discussion of the LSV data, the pH of the bulk solution (pH = 6.8) is used to calculate these RHE voltages. However, the pH at the Cu-membrane interface is much less than 6.8 due to the acidity of Nafion, which shifts the applied voltage more negative vs. RHE.

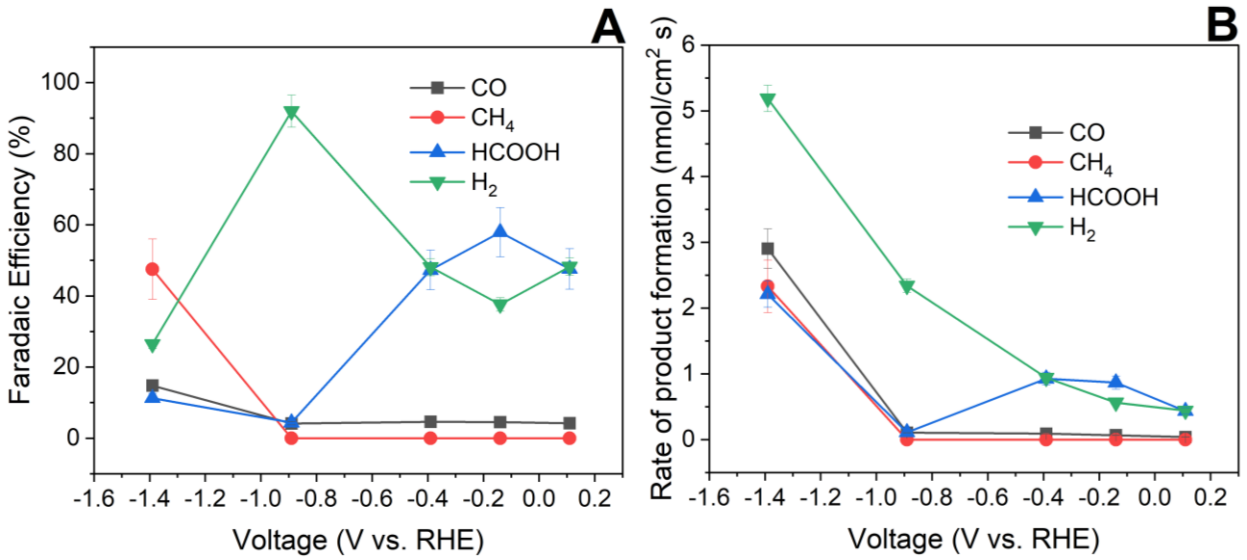

FIGURE 5. Faradaic efficiencies (A) and rate of formation (B) over the 1 hour experiment for formate, CO, and CH_4 produced from 52 wt. % PVDF in Nafion modified Cu at different voltages.

With increasing concentrations of PVDF and therefore increasing thickness of the polymer overlayer, mass transport of CO_2 to the electrode surface becomes limited because PVDF is less permeable to CO_2 than Nafion. Therefore, we performed mass transport calculations to determine when the concentration of PVDF in the overlayer limits reaction kinetics (Supporting Information, Mass Transport Calculations and Table S3). By calculating the flux of CO_2 through the PVDF-Nafion overlayers, CO_2 flux is compared against the rate of CO_2 consumed by the electrode. From these calculations, we find that more than 56 wt. % PVDF in the overlayer causes CO_2 mass transport to become the rate-determining step. However, a Cu electrode modified with 52 wt. % PVDF in Nafion at -0.14 V vs. RHE gives a reasonably high formate yield (58%). This yield of a formate is fairly high for a Cu-based catalyst, and most previous works use other metals to produce high formate yields such as 81% and 98%. There is some literature precedent, however, for Cu-based catalysts that achieve high formate yields including a Cu-Au catalyst that produces formate at a 81% Faradaic efficiency at -0.4 V vs. RHE.[59] Cu_2O nanoparticle films also generated formate at 98% Faradaic efficiency under high pressure ($\geq$ 45 atm) at -0.64 V vs. RHE. The authors of this work also found that at more negative potentials formate decreased.[60] Comparing our work to previous studies, it seems that formate production is favored at lower voltages, especially around from -0.4 to -0.6 V vs. RHE.

After modifying Cu electrodes with PVDF-Nafion polymer overlayers, we tested the effect of controlling proton availability in the reaction electrolyte. By adding an aprotic solvent (acetonitrile) to the bicarbonate electrolyte, the total proton concentration in the electrolyte is decreased with increasing concentrations of acetonitrile. With a decrease in proton availability, we hypothesize that the M-CO intermediate is less likely to be protonated to generate CH_4 and is more prone to undergo M-CO coupling to generate C2 and C3 products. Two control experiments

verified that acetonitrile vapor is not artificially contributing to CO, CH_4, or C_2H_4 yields during GC measurements. When no voltage is applied in a 75 wt. % acetonitrile/bicarbonate electrolyte to an unmodified Cu electrode or a Cu electrode modified with 15 μm of Nafion, under both flowing and static CO_2 during the reaction, no carbon-containing products were detected. A Cu electrode in 75 wt. % acetonitrile/pH 7 phosphate buffer at -0.89 V vs. RHE with no CO_2 flowing also did not generate any carbon-containing products. These control experiments verify that acetonitrile is chemically stable under relevant experimental conditions, and it is neither electrochemically breaking down nor reacting with CO_2/bicarbonate to make CO_2 reduction products.

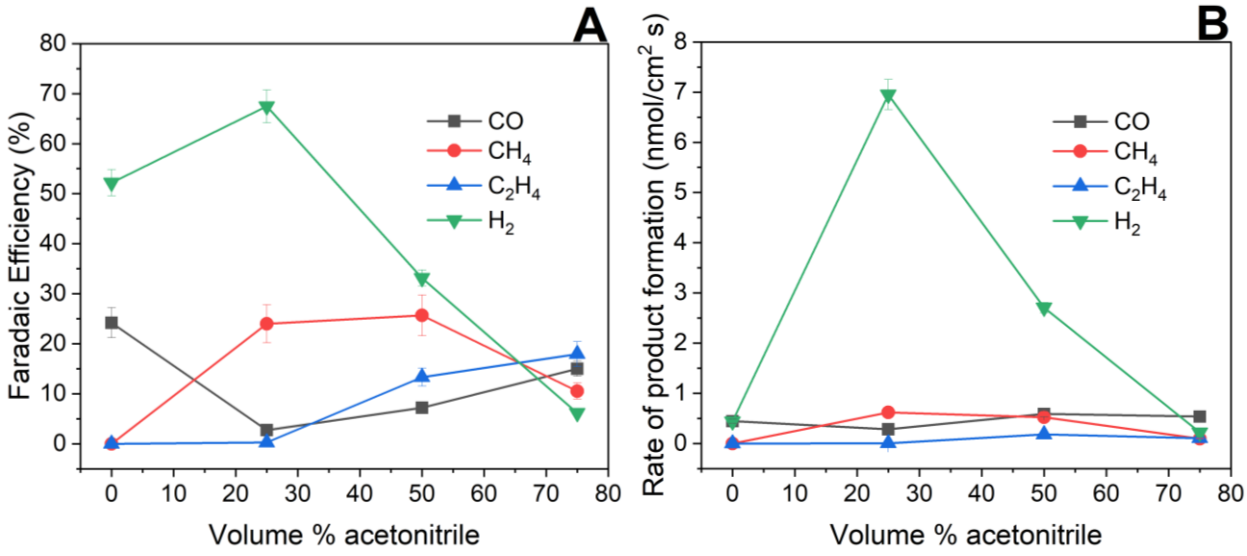

FIGURE 6. Faradaic efficiencies (A) and rate of formation (B) over the 1 hour experiment for gas products generated from unmodified Cu in acetonitrile/bicarbonate electrolyte at -0.89 V vs. RHE.

Fig. 6 presents the gas products generated from an unmodified Cu electrode in 0-75 vol. % acetonitrile in bicarbonate electrolytes at -0.89 V vs. RHE. At 0% acetonitrile, CO is the only gas product. Adding increasing amounts of acetonitrile causes the Faradaic efficiencies for CO production to decrease and then increase slightly, but the CO yield is never as high as in 0% acetonitrile (Fig. 6A). These results signify that acetonitrile hinders CO production. With

increasing amounts of acetonitrile, CH_4 and C_2H_4 are generated. This trend means that while the M-CO intermediate is still protonated to produce CH_4, M-CO and M-CO are also dimerizing to produce C_2H_4. The observation that the C_2H_4 yield continuously increases with increasing acetonitrile shows that decreasing proton availability promotes dimerization of the M-CO intermediate. The partial charge densities and rate of formations follow similar trends as the Faradaic efficiencies (Fig. S6 and Fig. 6B).

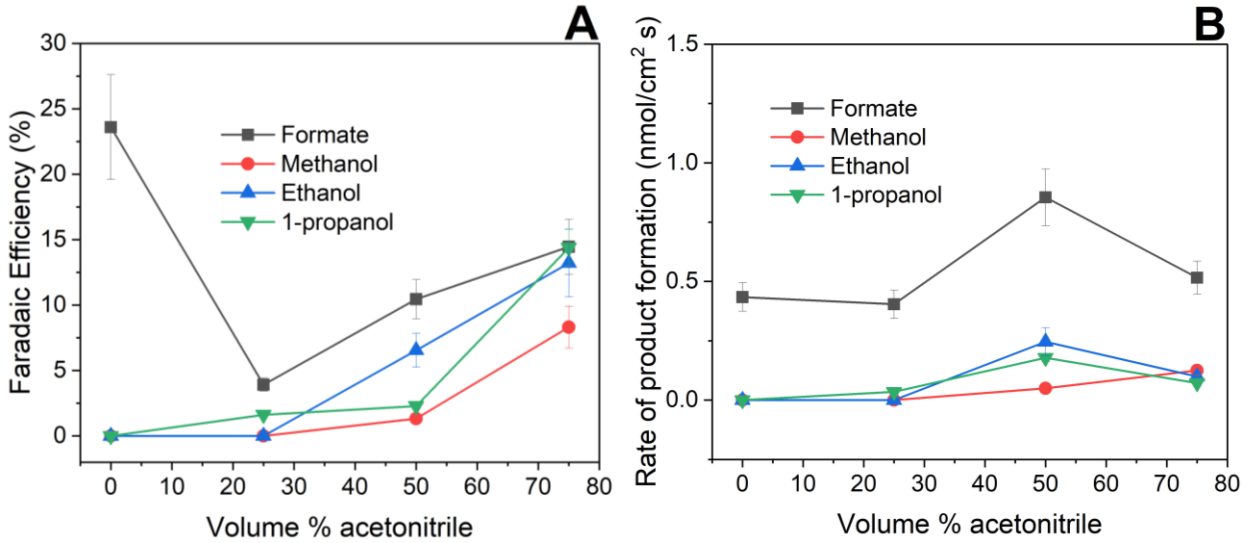

FIGURE 7. Faradaic efficiencies (A) and rate of formation (B) over the 1 hour experiment for liquid products generated from unmodified Cu in acetonitrile/bicarbonate electrolyte at -0.89 V vs. RHE.

Fig. 7 shows the liquid products generated from the abovementioned electrodes under the same reaction conditions. Similar to CO production, formate production is also favored in 0% acetonitrile, and production decreases with increasing amounts of acetonitrile (Fig. 7A). Alcohol production increases with increasing concentrations of acetonitrile, and the M-CO intermediate dimerizes and trimerizes to produce ethanol and 1-propanol. Interestingly, the partial charge density and rate of product formation are highest at 50 vol. % acetonitrile (Fig. S7 and Fig. 7B).

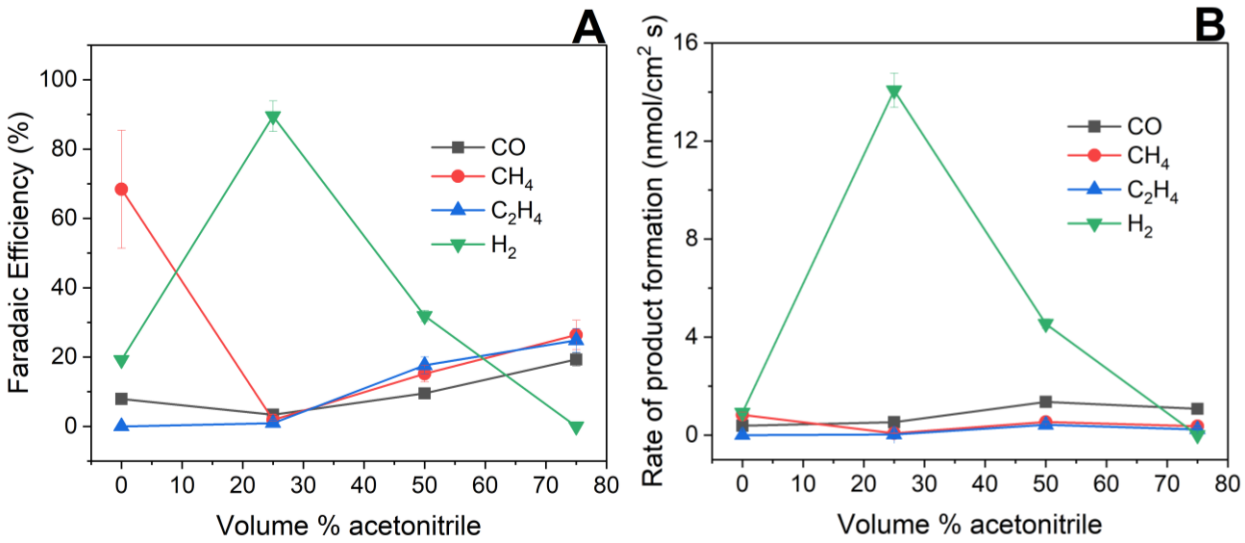

FIGURE 8. Faradaic efficiencies (A) and rate of formation (B) over the 1 hour experiment for gas products produced from Cu modified with 15 µm Nafion overlayer in acetonitrile/bicarbonate electrolyte at -0.89 V vs. RHE.

Fig. 8 presents the gas products generated from a Cu electrode modified with a 15 µm Nafion overlayer in 0-75 vol. % acetonitrile in bicarbonate electrolyte at -0.89 V vs. RHE. CO production has a different trend than the unmodified Cu electrode in that increasing the amount of acetonitrile also slightly increases CO production. CH_4 production is severely hindered because in an electrolyte without acetonitrile, the Nafion overlayer stabilizes the M-CO intermediate and subsequently allows for its rapid protonation to generate CH_4. With increasing amounts of acetonitrile, protonation of the M-CO intermediate is slowed and dimerization to produce C_2H_4 is enhanced (Fig. 8A). As for the unmodified Cu electrode, the partial charge density and rate of product formation is highest at 50 vol. % acetonitrile (Fig. S8 and Fig. 8B).

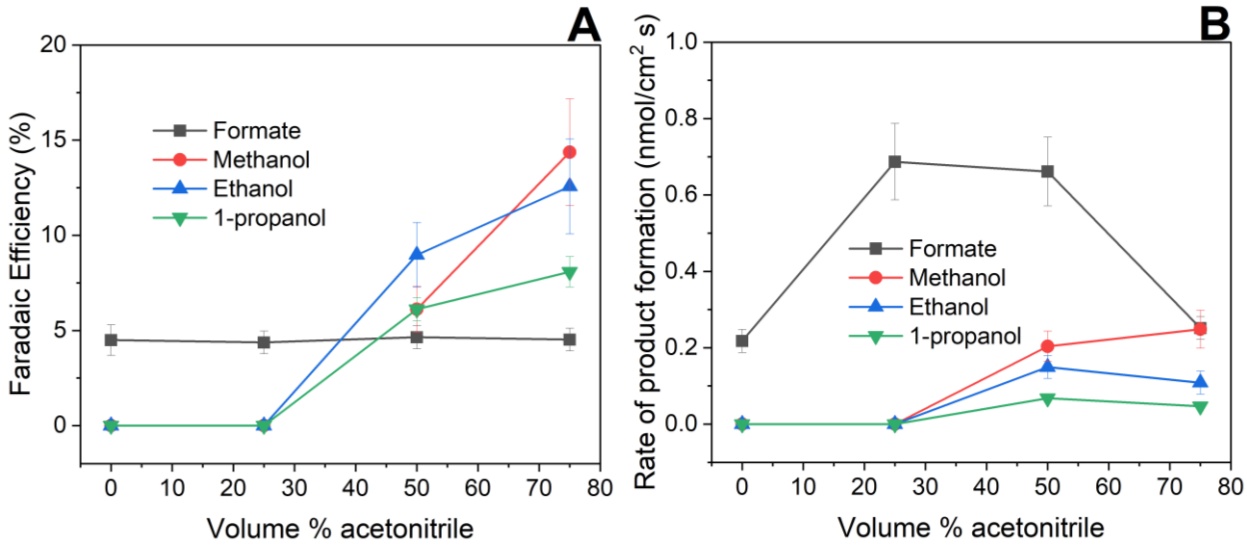

FIGURE 9. Faradaic efficiencies (A) and rate of formation (B) over the 1 hour experiment for liquid products produced from Cu modified with 15 µm Nafion overlayer in acetonitrile/bicarbonate electrolyte at -0.89 V vs. RHE.

Fig. 9 shows the liquid products generated from the same electrodes under the same reaction conditions. The Faradaic efficiencies for formate production remain nearly constant with changing electrolyte composition, while alcohol production increases with increasing acetonitrile. Partial charge density analysis (Fig. S9) shows that formate has the highest partial charge density at 25 vol. % acetonitrile, ethanol and 1-propanol have the highest partial charge densities at 50 vol. % acetonitrile, and methanol has the highest partial charge density at 75 vol. % acetonitrile. Formate production on a molar basis is highest for all of the electrodes because formate is only a 2 e^- product, while the other liquid products are more highly reduced.

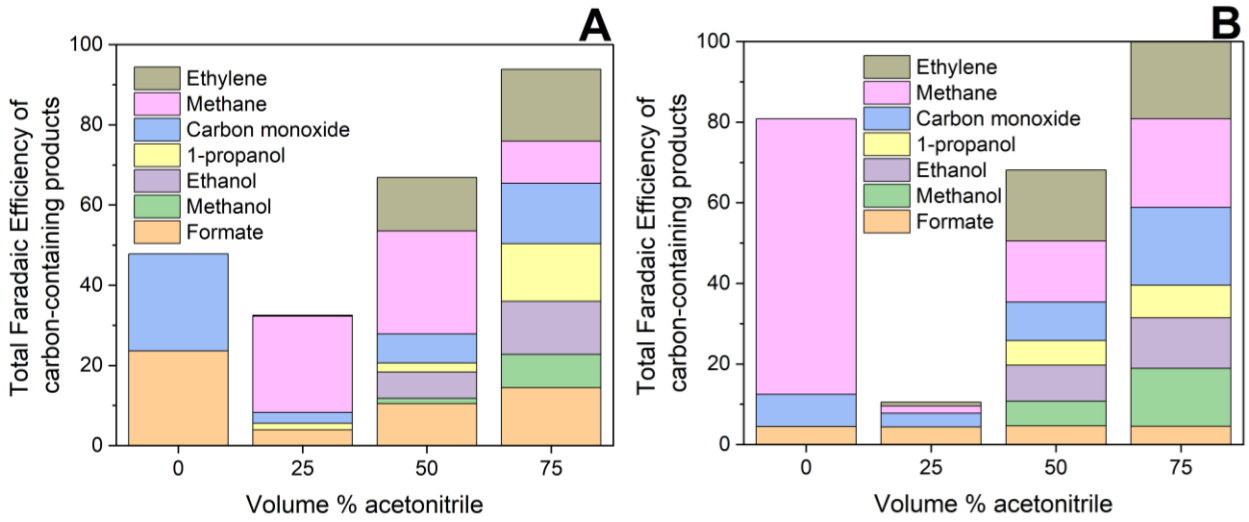

FIGURE 10. Total carbon-containing products generated from unmodified Cu electrode (A) and Cu electrode modified with 15 µm Nafion overlayer (B) in varying concentrations of acetonitrile in the bicarbonate electrolyte at -0.89 V vs. RHE.

Fig. 10 compares the total carbon-containing products produced from an unmodified Cu electrode and a Cu electrode modified with 15 µm Nafion overlayer in varying volume percents of acetonitrile. On an unmodified Cu electrode, at 0% acetonitrile, only formate and CO are produced. At the same voltage and reaction conditions, a Cu electrode modified with 15 µm Nafion produces a large amount of CH_4 due to the stabilization of the M-CO intermediate and rapid protonation of this intermediate. At 25 vol. % acetonitrile, the unmodified Cu electrode generates 24% CH_4 yet the Nafion-modified Cu electrodes only generates 2% CH_4. This difference means that M-CO is readily protonated with Cu, but not with Nafion-Cu when 25% acetonitrile is present. At 50 vol. % acetonitrile, still more CH_4 is made on the Cu surface as compared to Nafion-Cu, but more C_2H_4 is made with Nafion-Cu. At 75 vol. % acetonitrile, more CH_4, C_2H_4, and CO are produced on the Nafion-Cu electrode, and the total carbon-containing product yields exceed that of unmodified Cu. Importantly, the total carbon-containing products with the electrodes containing the 75 vol. % acetonitrile is nearly 100%, indicating that the H_2 evolution side reaction is almost completely avoided in these cases.

Fig. 11 displays two schemes for CO_2 reduction to formate and ethylene. A Cu electrode modified with 52 wt. % PVDF in Nafion overlayer creates a hydrophobic environment in which producing water is unfavorable. Since formate is the only CO_2 reduction product in which water is not produced concomitantly, a hydrophobic electrode favors formate production. The pathway to formate is relatively simple in which only one intermediate is formed and requires two protons and two electrons (Fig. 11A). The intermediate is an oxygen-bound M-OCHO species that can be converted to HCOOH either through a proton-coupled electron transfer step or sequential electron and proton transfer.[63] When the total proton concentration is decreased in the reaction electrolyte, the rate of protonation of the M-CO intermediate decreases, which causes a decrease in CH_4 production. M-CO coupling chemistry is facilitated by acetonitrile (which decreases proton availability and hence proton transfer kinetics), but not by the hydrophobicity of the polymer overlayer (Fig. 11B).

We note that the current densities of the systems described in this work are lower than those of other reported works that utilize nanostructured and gas-diffusion electrodes.[17,61,62] This manuscript focuses on the underlying effects of polymer overlayers on CO_2 reduction, and we chose to utilize flat electrodes to keep the systems as simple as possible. In future work, we will explore the effect of polymer overlayers on CO_2 reduction catalysts that possess greater current densities.

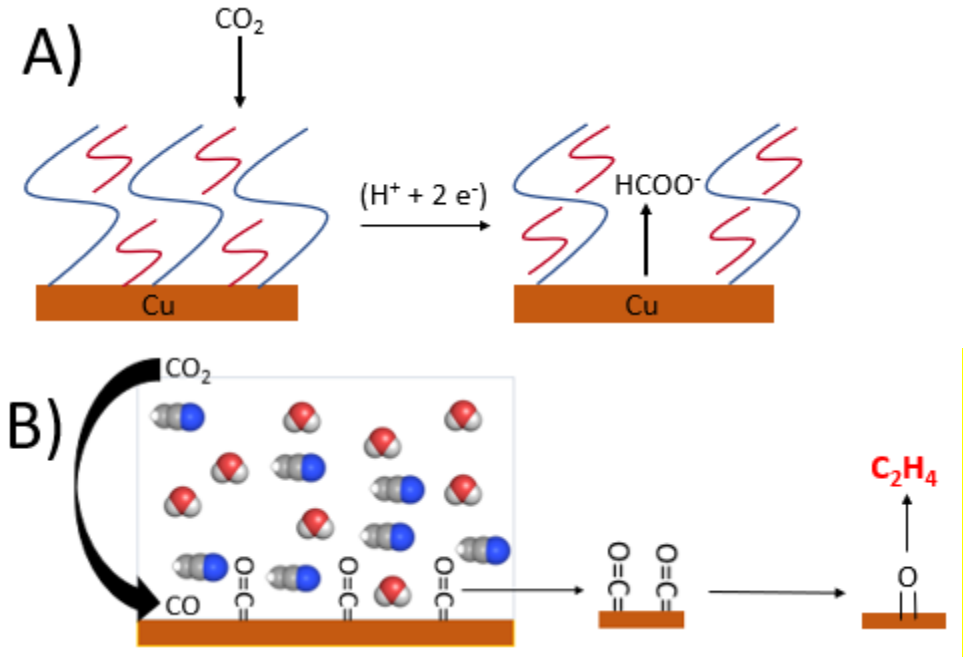

FIGURE 11. Schematic of high formate production using Cu modified by 52 wt. % PVDF in Nafion polymer overlayer (A). The blue curved lines represent Nafion and the red curved lines represent PVDF. In this hydrophobic environment, formate is the preferred product because formate is the only CO_2 reduction product that does not generate water, and generating water is unfavorable in a hydrophobic environment. Schematic of ethylene formation on a Cu electrode in an acetonitrile/bicarbonate electrolyte (B). Adding an aprotic solvent decreases the total proton concentration, which subsequently decreases the rate of M-CO protonation. This aprotic environment promotes M-CO coupling to generate C2 and C3 products (ethylene production is shown as one example) instead of protonating M-CO to generate CH_4.

Conclusion

In conclusion, this work demonstrates that controlling the hydrophobicity of the electrode and proton availability of the electrolyte strongly dictates the production of different CO_2 reduction products. Formate production is favored by a hydrophobic electrode, however, too much hydrophobicity causes mass transport issues because hydrophobic PVDF is less permeable towards CO_2. The decrease in proton concentration slows down the protonation of the M-CO intermediate to generate CH_4, but promotes M-CO and M-CO coupling chemistry to produce C2 and C3 products. This control of hydrophobicity by using polymer blends and mixed aprotic-protic solvent

systems is a facile and effective method to tune the selectivity of CO_2 reduction catalysts that can be applied to many different catalyst architectures.

Associated Content

Supporting information

The Supporting Information is available free of charge on the ACS Publications website.

Mass transport calculations, partial charge density calculations, electrochemical impedance spectroscopy data, contact angle measurements, and additional chronoamperometry data.

Author Information

Corresponding Author

*E-mail: cbarile@unr.edu

Notes

The authors declare no competing financial interest.

Acknowledgements

This material is based upon work supported by the National Science Foundation CAREER Award under Grant No. CHE-2046105. We acknowledge the Shared Instrumentation Laboratory in the Department of Chemistry at UNR. We also acknowledge Dr. Joel DesOrmeau and the Mackay Microbeam Laboratory at UNR for support of the SEM-EDS analysis.

References

1. Zhao, J.; Xue, S.; Barber, J.; Zhou, Y.; Meng, J.; Ke, X. An overview of Cu-based heterogeneous electrocatalysts for CO_2 reduction. *J. Mater. Chem. A,* **2020**, *8*, 4700-4734.
2. Chen, X.; Henckel, D. A.; Nwabara, Y. O.; Li, Y.; Frenkel, A. I.; Fister, T. T.; Kenis, P. J. A.; Gewirth, A. A. Controlling Speciation during CO_2 Reduction on Cu-Alloy Electrodes. *ACS Catal.,* **2020**, *10*, 672-682.
3. Chen, Y.; Fan, Z.; Wang, J.; Ling, C.; Niu, W.; Huang, Z.; Liu, G.; Chen, B.; Lai, Z.; Liu, X.; Li, B.; Zong, Y.; Gu, L.; Wang, J.; Wang, X.; Zhang, H. Ethylene Selectivity in Electrocatalytic CO_2 Reduction on Cu Nanomaterials: A Crystal Phase-Dependent Study. *J. Am. Chem. Soc.,* **2020**, *142*, 12760-12766.

4. Zhu, Q.; Sun, X.; Yang, D.; Ma, J.; Kang, X.; Zheng, L.; Zhang, J.; Wu, Z.; Han, B. Carbon dioxide electroreduction to C2 products over copper-cuprous oxide derived from electrosynthesized copper complex. *Nat. Commun.,* **2019**, *10*, 3851.
5. Kim, D.; Kley, C. S.; Li, Y.; Yang, P. Copper nanoparticle ensembles for selective electroreduction of CO_2 to C2-C3 products. *Proc. Natl. Acad. Sci.,* **2017**, *114*, 10560.
6. Handoko, A. D.; Ong, C. W.; Huang, Y.; Lee, Z. G.; Lin, L.; Panetti, G. B.; Yeo, B. S. Mechanistic Insights into the Selective Electroreduction of Carbon Dioxide to Ethylene on Cu_2O-Derived Copper Catalysts. *J. Phys. Chem. C.,* **2016**, *120*, 20058-20067.
7. Huang, Y.; Handoko, A. D.; Hirunsit, P.; Yeo, B. S. Electrochemical Reduction of CO_2 Using Copper Single-Crystal Surfaces: Effects of CO* Coverage on the Selective Formation of Ethylene. *ACS Catal.,* **2017**, *7*, 1749-1756.
8. Dutta, A.; Rahaman, M.; Mohos, M.; Zanetti, A.; Broekmann, P. Electrochemical CO_2 Conversion Using Skeleton (Sponge) Type of Cu Catalysts. *ACS Catal.,* **2017**, 7, 5431-5437.
9. Reller, C.; Krause, R.; Volkova, E.; Schmid, B.; Neubauer, S.; Rucki, A.; Schuster, M.; Schmid, G. Selective Electroreduction of CO_2 toward Ethylene on Nano Dendritic Copper Catalysts at High Current Density. *Adv. Energy Mater.,* **2017**, 7, 1602114.
10. Yang, K. D.; Ko, W. R.; Lee, J. H.; Kim, S. J.; Lee, H.; Lee, M. H.; Nam, K. T. Morphology-Directed Selective Production of Ethylene or Ethane from CO_2 on a Cu Mesopore Electrode. *Angew. Chem. Int. Ed.,* **2017**, 56, 796-800.
11. Baturina, O. A.; Lu, Q.; Padilla, M. A.; Xin, L.; Li, W.; Serov, A.; Artyushkova, K.; Atanassov, P.; Xu, F.; Epshteyn, A.; Brintlinger, T.; Schuette, M.; Collins, G. E. CO_2 Electroreduction to Hydrocarbons on Carbon-Supported Cu Nanoparticles. *ACS Catal.,* **2014**, 4, 3682-3695.
12. Wu, D.; Dong, C.; Wu, D.; Fu, J.; Liu, H.; Hu, S.; Jiang, Z.; Qiao, S. Z.; Du, X.-W. Cuprous ions embedded in ceria lattice for selective and stable electrochemical reduction of carbon dioxide to ethylene. *J. Mater. Chem. A.,* **2018**, 6, 9373-9377.
13. Pang, Y.; Burdyny, T.; Dinh, C.-T.; Kibria, M. G.; Fan, J. Z.; Liu, M.; Sargent, E. H.; Sinton, D. Joint tuning of nanostructured Cu-oxide morphology and local electrolyte programs high-rate CO_2 reduction to C_2H_4. *Green Chem.,* **2017**, 19, 4023-4030.
14. Ma, W.; Xie, S.; Liu, T.; Fan, Q.; Ye, J.; Sun, F.; Jiang, Z.; Zhang, Q.; Cheng, J.; Wang, Y. Electrocatalytic reduction of CO_2 to ethylene and ethanol through hydrogen-assisted C–C coupling over fluorine-modified copper. *Nat. Catal.,* **2020**, 3, 478-487.
15. Kuhl, K. P.; Cave, E. R.; Abram, D. N.; Jaramillo T. F. New insights into the electrochemical reduction of carbon dioxide on metallic copper surfaces. *Energy Environ. Sci.,* **2012**, 5, 7050-7059.
16. Vasileff, A.; Zhi, X.; Xu, C.; Ge, L.; Jiao, Y.; Zheng, Y.; Qiao, S.-Z. Selectivity Control for Electrochemical CO_2 Reduction by Charge Redistribution on the Surface of Copper Alloys. *ACS Catal.,* **2019**, 9, 9411-9417.
17. García de Arquer, F. P.; Dinh, C.-T.; Ozden, A.; Wicks, J.; McCallum, C.; Kirmani, A. R.; Nam, D.-H.; Gabardo, C.; Seifitokaldani, A.; Wang, X.; Li, Y. C.; Li, F.; Edwards, J.; Richter, L. J.; Thorpe, S. J.; Sinton, D.; Sargent, E. H. CO_2 electrolysis to multicarbon products at activities greater than 1 A cm^{-2}. *Science* **2020**, 367, 661-666.
18. Hori, Y.; Kikuchi, K.; Suzuki, S. Production of CO and CH_4 in electrochemical reduction of CO_2 at metal electrodes in aqueous hydrogencarbonate solution. *Chem. Lett.* **1985**, 14, 1695-1698.
19. Janáky, C.; Hursán, D.; Endrődi, B.; Chanmanee, W.; Roy, D.; Liu, D.; de Tacconi, N. R.; Dennis, B. H.; Rajeshwar, K. Electro- and Photoreduction of Carbon Dioxide: The Twain Shall Meet at Copper Oxide/Copper Interfaces. *ACS Energy Lett.* **2016**, *1*, 332-338.

20. Sander, R. Compilation of Henry's law constants, version 3.99. *Atmos. Chem. Phys. Discuss.* **2014**, *14*, 29615-30521.
21. da Silva, A. H. M.; Raaijman, S. J.; Santana, C. S.; Assaf, J. M.; Gomes, J. F.; Koper, M. T. M. Electrocatalytic CO_2 reduction to C2+ products on Cu and CuxZny electrodes: Effects of chemical composition and surface morphology. *J. Electroanal. Chem.* **2021**, *880*, 114750.
22. Wang, X.; Klingan, K.; Klingenhof, M.; Möller, T.; Ferreira de Araújo, J.; Martens, I.; Bagger, A.; Jiang, S.; Rossmeisl, J.; Dau, H.; Strasser, P. Morphology and mechanism of highly selective Cu(II) oxide nanosheet catalysts for carbon dioxide electroreduction. *Nat. Commun.,* **2021**, *12*, 794.
23. Dutta, A.; Rahaman, M.; Luedi, N. D.; Mohos, M.; Broekmann, P. Morphology Matters: Tuning the Product Distribution of CO_2 Electroreduction on Oxide-Derived Cu Foam Catalysts. *ACS Catal.,* **2016**, *6*, 3804-3814.
24. Suen, N.-T.; Kong, Z.-R.; Hsu, C.-S.; Chen, H.-C.; Tung, C.-W.; Lu, Y.-R.; Dong, C.-L.; Shen, C.-C.; Chung, J.-C.; Chen, H. M. Morphology Manipulation of Copper Nanocrystals and Product Selectivity in the Electrocatalytic Reduction of Carbon Dioxide. *ACS Catal.,* **2019**, *9*, 5217-5222.
25. Fan, M.; Bai, Z.; Zhang, Q.; Ma, C.; Zhou, X.-D.; Qiao, J. Aqueous CO_2 reduction on morphology controlled CuxO nanocatalysts at low overpotential. *RSC Adv.,* **2014**, *4*, 44583-44591.
26. Igarashi, R.; Takeuchi, R.; Kubo, K.; Mizuta, T.; Kume, S. On-Surface Modification of Copper Cathodes by Copper(I)-Catalyzed Azide Alkyne Cycloaddition and CO_2 Reduction in Organic Environments. *Front. Chem.,* **2019**, *7*, 1-10.
27. Xie, M. S.; Xia, B. Y.; Li, Y.; Yan, Y.; Yang, Y.; Sun, Q.; Chan, S. H.; Fisher, A.; Wang, X. Amino acid modified copper electrodes for the enhanced selective electroreduction of carbon dioxide towards hydrocarbons. *Energy Environ. Sci.,* **2016**, *9*, 1687-1695.
28. Wang, J.; Zhang, F.; Kang, X.; Chen, S. Organic functionalization of metal catalysts: Enhanced activity towards electroreduction of carbon dioxide. *Curr. Opin. Electrochem.,* **2019**, *13*, 40-46.
29. Zhou, Y.; Che, F.; Liu, M.; Zou, C.; Liang, Z.; De Luna, P.; Yuan, H.; Li, J.; Wang, Z.; Xie, H.; Li, H.; Chen, P.; Bladt, E.; Quintero-Bermudez, R.; Sham, T.-K.; Bals, S.; Hofkens, J.; Sinton, D.; Chen, G.; Sargent, E. H., Dopant-induced electron localization drives CO_2 reduction to C2 hydrocarbons. *Nat. Chem.,* **2018**, *10*, 974-980.
30. Morales-Guio, C. G.; Cave, E. R.; Nitopi, S. A.; Feaster, J. T.; Wang, L.; Kuhl, K. P.; Jackson, A.; Johnson, N. C.; Abram, D. N.; Hatsukade, T.; Hahn, C.; Jaramillo, T. F. Improved CO_2 reduction activity towards C2+ alcohols on a tandem gold on copper electrocatalyst. *Nat. Catal.,* **2018**, *1*, 764-771.
31. Ye, K.; Cao, A.; Shao, J.; Wang, G.; Si, R.; Ta, N.; Xiao, J.; Wang, G. Synergy effects on Sn-Cu alloy catalyst for efficient CO_2 electroreduction to formate with high mass activity. *Sci. Bull.,* **2020**, *65*, 711-719.
32. Zheng, X.; Ji, Y.; Tang, J.; Wang, J.; Liu, B.; Steinrück, H.-G.; Lim, K.; Li, Y.; Toney, M. F.; Chan, K.; Cui, Y. Theory-guided Sn/Cu alloying for efficient CO_2 electroreduction at low overpotentials. *Nat. Catal.,* **2019**, *2*, 55-61.
33. Wang, L.; Higgins, D. C.; Ji, Y.; Morales-Guio, C. G.; Chan, K.; Hahn, C.; Jaramillo, T. F. Selective reduction of CO to acetaldehyde with CuAg electrocatalysts. *Proc. Natl. Acad. Sci.,* **2020**, *117*, 12572.
34. Sa, Y. J.; Lee, C. W.; Lee, S. Y.; Na, J.; Lee, Y.; Hwang, Y. J. Catalyst–electrolyte interface chemistry for electrochemical CO_2 reduction. *Chem. Soc. Rev.,* **2020**, *49*, 6632-6665.
35. Moura de Salles Pupo, M.; Kortlever, R. Electrolyte Effects on the Electrochemical Reduction of CO_2. *ChemPhysChem,* **2019**, *20*, 2926-2935.

36. Bondue, C. J.; Graf, M.; Goyal, A.; Koper, M. T. M. Suppression of Hydrogen Evolution in Acidic Electrolytes by Electrochemical CO_2 Reduction. *J. Am. Chem. Soc.,* **2021**, *143*, 279-285.
37. Varela, A. S.; Kroschel, M.; Reier, T.; Strasser, P. Controlling the selectivity of CO_2 electroreduction on copper: The effect of the electrolyte concentration and the importance of the local pH. *Catal. Today,* **2016**, *260*, 8-13.
38. Jiang, C.; Nichols, A. W.; Walzer, J. F.; Machan, C. W. Electrochemical CO_2 Reduction in a Continuous Non-Aqueous Flow Cell with $[Ni(cyclam)]^{2+}$. *Inorg. Chem.,* **2020**, *59*, 1883-1892.
39. Oh, Y.; Vrubel, H.; Guidoux, S.; Hu, X. Electrochemical reduction of CO_2 in organic solvents catalyzed by MoO_2. *Chem. Commun.,* **2014**, *50*, 3878-3881.
40. Díaz-Duque, A.; Sandoval-Rojas, A. P.; Molina-Osorio, A. F.; Feliu, J. M.; Suárez-Herrera, M. F. Electrochemical reduction of CO_2 in water-acetonitrile mixtures on nanostructured Cu electrode. *Electrochem. Commun.,* **2015**, *61*, 74-77.
41. Figueiredo, M. C.; Ledezma-Yanez, I.; Koper, M. T. M. In Situ Spectroscopic Study of CO_2 Electroreduction at Copper Electrodes in Acetonitrile. *ACS Catal.,* **2016**, *6*, 2382-2392.
42. Desilvestro, J. Pons, S. The cathodic reduction of carbon dioxide in acetonitrile: An electrochemical and infrared spectroelectrochemical study. *J. Electroanal. Chem. Interf. Electrochem.,* **1989**, *267*, 207-220.
43. Pan, H.; Barile, C. J. Electrochemical CO_2 reduction to methane with remarkably high Faradaic efficiency in the presence of a proton permeable membrane. *Energy Environ. Sci.,* **2020**, *13*, 3567-3578.
44. Gautam, R. P.; Lee, Y. T.; Herman, G. L.; Moreno, C. M.; Tse, E. C. M.; Barile, C. J. Controlling Proton and Electron Transfer Rates to Enhance the Activity of an Oxygen Reduction Electrocatalyst. *Angew. Chem. Int. Ed.,* **2018**, *57*, 13480-13483.
45. Mennel, J. A.; Pan, H.; Palladino, S. W.; Barile, C. J. Electrocatalytic CO_2 Reduction by Self-Assembled Monolayers of Metal Porphyrins. *J. Phys. Chem. C.,* **2020**, *124*, 19716-19724.
46. Dinh, C.-T.; Burdyny, T.; Kibria, M. G.; Seifitokaldani, A.; Gabardo, C. M.; García de Arquer, F. P.; Kiani, A.; Edwards, J. P.; De Luna, P.; Bushuyev, O. S.; Zou, C.; Quintero-Bermudez, R.; Pang, Y.; Sinton, D.; Sargent, E. H. CO_2 electroreduction to ethylene via hydroxide-mediated copper catalysis at an abrupt interface. *Science.* **2018**, *360*, 783.
47. Huo, Y.; Peng, X.; Liu, X.; Li, H.; Luo, J. High Selectivity Toward C_2H_4 Production over Cu Particles Supported by Butterfly-Wing-Derived Carbon Frameworks. *ACS Appl. Mater. Interfaces.,* **2018**, *10*, 12618-12625.
48. Mistry, H.; Varela, A. S.; Bonifacio, C. S.; Zegkinoglou, I.; Sinev, I.; Choi, Y.-W.; Kisslinger, K.; Stach, E. A.; Yang, J. C.; Strasser, P.; Cuenya, B. R. Highly selective plasma-activated copper catalysts for carbon dioxide reduction to ethylene. *Nat. Commun.,* **2016**, *7*, 12123.
49. Checco, A.; Hofmann, T.; DiMasi, E.; Black, C. T.; Ocko, B. M. Morphology of Air Nanobubbles Trapped at Hydrophobic Nanopatterned Surfaces. *Nano Lett.,* **2010**, *10*, 1354-1358.
50. Melnichenko, Y. B.; Lavrik, N. V.; Popov, E.; Bahadur, J.; He, L.; Kravchenko, I. I.; Smith, G.; Pipich, V.; Szekely, N. K. Cavitation on Deterministically Nanostructured Surfaces in Contact with an Aqueous Phase: A Small-Angle Neutron Scattering Study. *Langmuir,* **2014**, *30*, 9985-9990.
51. Sakamoto, N.; Arai, T. Enhanced electrochemical CO_2 reduction selectivity by application of self-assembled polymer microparticles to a silver electrode. *Chemical Commun.,* **2019**, *55*, 11623-11625.
52. Buckley, A. K.; Lee, M.; Cheng, T.; Kazantsev, R. V.; Larson, D. M.; Goddard III, W. A.; Toste, F. D.; Toma, F. M. Electrocatalysis at Organic–Metal Interfaces: Identification of

Structure–Reactivity Relationships for CO_2 Reduction at Modified Cu Surfaces. *J. Am. Chem. Soc.,* **2019**, *141*, 7355-7364.
53. Li, J.; Chen, G.; Zhu, Y.; Liang, Z.; Pei, A.; Wu, C.-L.; Wang, H.; Lee, H. R.; Liu, K.; Chu, S.; Cui, Y. Efficient electrocatalytic CO_2 reduction on a three-phase interface. *Nat. Catal.,* **2018**, *1*, 592-600.
54. Wakerley, D.; Lamaison, S.; Ozanam, F.; Menguy, N.; Mercier, D.; Marcus, P.; Fontecave, M.; Mougel, V. Bio-inspired hydrophobicity promotes CO_2 reduction on a Cu surface. *Nat. Mater.,* **2019**, *18*, 1222-1227.
55. Zhao, X.; Du, L.; You, B.; Sun, Y. Integrated Design for Electrocatalytic Carbon Dioxide Reduction. *Catal. Sci. Technol*., **2020**, 10, 2711-2720.
56. Kreuer, K. D. I. M.; Fuchs, A.; Maier J. Proton and Water Transport in Nano-separated Polymer Membranes. *J. Phys. IV*, **2000**, *10* , 279-281.
57. Pan, H.; Barile, C. J. Bifunctional nickel and copper electrocatalysts for CO_2 reduction and the oxygen evolution reaction. *J. Mater. Chem. A.,* **2020**, *8*, 1741-1748.
58. Buckley, A. K.; Lee, M.; Cheng, T.; Kazantsev, R. V.; Larson, D. M.; Goddard, W. A.; Toste, F. D.; Toma, F. M. Electrocatalysis at Organic-Metal Interfaces: Identification of Structure-Reactivity Relationships for CO_2 Reduction at Modified Cu Surfaces. *J. Am. Chem. Soc.*, **2019**, *141*, 7355-7364.
59. Tao, Z.; Wu, Z.; Yuan, X.; Wu, Y.; Wang, H. Copper–Gold Interactions Enhancing Formate Production from Electrochemical CO_2 Reduction. *ACS Catal.,* **2019**, *9*, 10894-10898.
60. Li, J.; Kuang, Y.; Meng, Y.; Tian, X.; Hung, W.-H.; Zhang, X.; Li, A.; Xu, M.; Zhou, W.; Ku, C.-S.; Chiang, C.-Y.; Zhu, G.; Guo, J.; Sun, X.; Dai, H., Electroreduction of CO_2 to Formate on a Copper-Based Electrocatalyst at High Pressures with High Energy Conversion Efficiency. *J. Am. Chem. Soc.,* **2020**, *142*, 7276-7282.
61. Chen, X.; Chen, J.; Alghoraibi, N. M.; Henckel, D. A.; Zhang, R.; Nwabara, U. O.; Madsen, K. E.; Kenis, P. J. A.; Zimmerman, S. C.; Gewirth, A. A. *Nat. Catal.*, **2021**, *4*, 20-27.
62. Larrazabal, G. O.; Ma, M.; Seger, B. A Comprehensive Approach to Investigate CO_2 Reduction Electrocatalysts at High Current Densities. *Acc. Mater. Res.*, **2021**, *2*, 220-229.
63. Zhao, S.; Li, S.; Guo, T.; Zhang, S.; Wang, J.; Wu, Y.; Chen. Y. Advances in Sn-Based Catalysts for Electrochemical CO_2 Reduction. *Nano-Micro Lett.*, **2019**, *11*, 1-19.

TOC Image

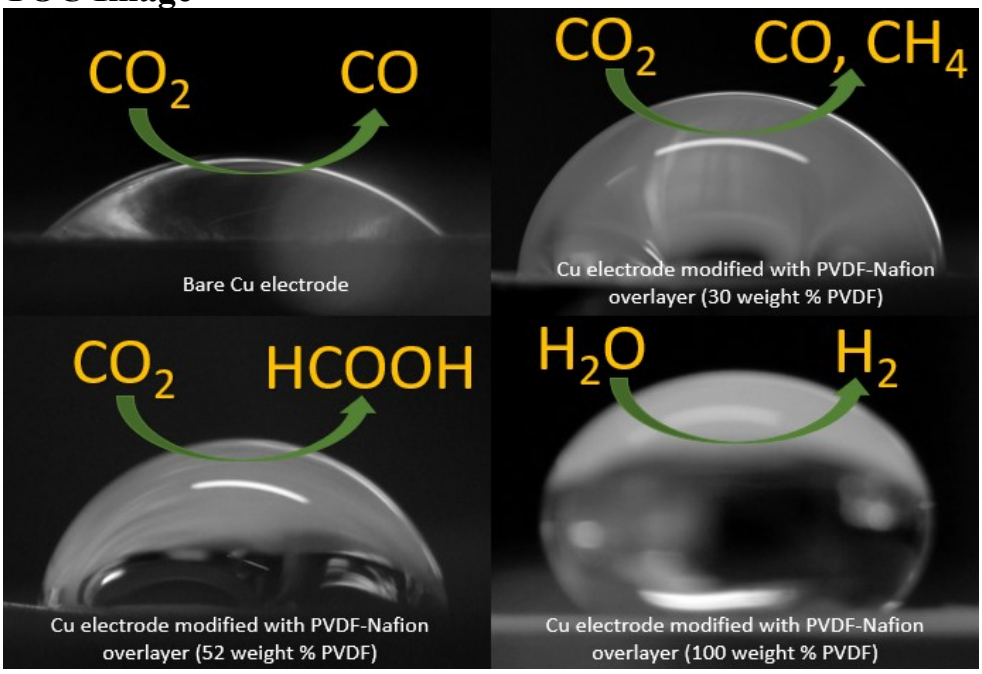
CO_2
CO
Bare Cu electrode
CO_2
CO, CH_4
Cu electrode modified with PVDF-Nafion overlayer (30 weight % PVDF)
CO_2
HCOOH
Cu electrode modified with PVDF-Nafion overlayer (52 weight % PVDF)
H_2O
H_2
Cu electrode modified with PVDF-Nafion overlayer (100 weight % PVDF)